Journal of Adhesion Science and Technology

ISSN: 0169-4243 (Print) 1568-5616 (Online) Journal homepage: http://www.tandfonline.com/loi/tast20

Viscoelastic, thermo-mechanical and environmental properties of composites based on polypropylene/poly(lactic acid) blend and copper modified nanoclay

Farida Bouzidi, Melia Guessoum, Magali Fois & Nacerddine Haddaoui

To cite this article: Farida Bouzidi, Melia Guessoum, Magali Fois & Nacerddine Haddaoui (2018) Viscoelastic, thermo-mechanical and environmental properties of composites based on polypropylene/poly(lactic acid) blend and copper modified nanoclay, Journal of Adhesion Science and Technology, 32:5, 496-515, DOI: 10.1080/01694243.2017.1365422

To link to this article: https://doi.org/10.1080/01694243.2017.1365422

JOURNAL OF ADHESION SCIENCE AND TECHNOLOGY, 2018
VOL. 32, NO. 5, 496–515
https://doi.org/10.1080/01694243.2017.1365422

Taylor & Francis
Taylor & Francis Group

Viscoelastic, thermo-mechanical and environmental properties of composites based on polypropylene/poly(lactic acid) blend and copper modified nanoclay

Farida Bouzidi[a], Melia Guessoum[a], Magali Fois[b] and Nacerddine Haddaoui[a]

[a]Laboratoire de Physico-Chimie des Hauts Polymères (LPCHP), Département de Génie des Procédés, Faculté de Technologie, Université Ferhat ABBAS Sétif-1, Sétif, Algeria; [b]Centre d'Etudes et de Recherche en Thermique, Environnement et Système (CERTES EA-3481), Université Paris Est Créteil, Créteil, France

ABSTRACT

Poly(lactic acid) (PLA)/polypropylene (PP) blends composites were prepared by incorporating 3 wt.% of copper modified montmorillonite (MMT-Cu^{2+}), obtained using cation exchange in a $CuSO_4$ solution, and 10 wt.% of polypropylene-graft-maleic anhydride (PP-g-MA) as a compatibilizer then varying the PLA content until 50 wt.%. These materials were subjected to several investigations such as X-rays diffraction, dynamic mechanical thermal analysis (DMTA), differential scanning calorimetry (DSC), scanning electron microscopy (SEM) and tensile and environmental tests. The DMTA analysis showed that the glassy PLA high stiffness and the PP crystalline phase compensate the decrease in the storage modulus occurring during the PP and PLA glass transitions, respectively. The variations of tan δ revealed no changes on the PP and PLA phases glass transitions temperatures which indicate the immiscibility of the two polymers, as supported by DSC analysis. Blends composites SEM micrographs stated the immiscibility of the system resulting in the poor adhesion of the PLA droplets to the PP matrix. Also, the blends composites exhibited intermediate tensile properties between those of PP and PLA. The incorporation of MMT-Cu^{2+} to the (50/50) PP/PLA blend accentuated its aptitude to water absorption and ensured an efficient antimicrobial activity over a satisfactorily long period of around six months.

ARTICLE HISTORY
Received 11 June 2017
Revised 1 August 2017
Accepted 2 August 2017

KEYWORDS
Polypropylene; poly(lactic acid); montmorillonite; composites; viscoelastic properties

1. Introduction

Poly(lactic acid) (PLA) is a linear biodegradable polyester that can be derived from renewable resources such as starch of crops like corn and sugar beet [1,2]. This polymer has a high transparency and elastic modulus, can be thermoplastically processed like conventional plastics, and is considered as a promising green material which should be widely used in the development of disposable products due to its biodegradability [3,4]. However, PLA presents several drawbacks resulting from its poor impact strength, small elongation at break, low heat deflection temperature (HDT) and high tendency to hydrolysis, which hinders its applicability in many commodity and technical fields [5].

CONTACT Melia Guessoum guessoum_melia@yahoo.fr

Among the modification techniques proposed to overcome the PLA limits, polymer blending has been considered as the more convenient and economical method to achieve materials with an advantageous combination of end-use properties [6,7]. Thus, blending PLA with soft and tough polymers was found to enhance mechanical properties without altering biodegradability [8]. In this context, blends of PLA with synthetic polymers such as low density polyethylene (LDPE) [9], linear low density polyethylene (LLDPE) [10] and polycarbonate (PC) [11] and biodegradable resins like thermoplastic starch (TPS) [12], poly(butylene succinate (PBS) [13] and poly(butylene adipate-co-terephthalate) (PBAT) [14] have been extensively studied.

Polypropylene (PP) is a useful commodity polymer with outstanding properties such as low density, sterilizability, excellent mechanical performances and high chemical resistance to many solvents, bases, and acids. Due to these characteristics, PP is used in a huge number of applications like home appliances, automotive parts and extruded profiles [15,16]. Additionally, PP presents an excellent good barrier to H_2O, but its relatively high permeability to O_2 limits its applications. In opposition, PLA has a significantly lower O_2 permeability but exhibits a poor barrier to H_2O, which is considered as a serious shortcoming towards many applications [17]. Consequently, blending of PP and PLA appears as an attractive combination to ensure complementarity between the two polymers and manufacture materials, especially for packaging industry. Thus, the PP/PLA blend has been an attractive topic for characterizing the system as a function of composition and promoting its performances via compatibilization processes and nanofillers incorporation [18–21]. In this context, Yoo et al. [18] investigated the effects of compatibilizers and hydrolysis on the mechanical properties, interfacial tension, and morphology of (80/20) PP/PLA blends. They found that maleic anhydride-grafted polypropylene (PP-g-MA) is an effective compatibilizer for improving the tensile strength and that maleated styrene ethylene/butylene-styrene (SEBS-g-MA) acts as an efficient impact-modifier. On the other hand, Pivsa-Art et al. [19] focused their work on PP/PLA blends with PP:PLA ratios of 80:20 and 20:80 prepared by injection molding process. They noticed an increase in the impact strength of the blends in presence of PP-g-MA as a compatibilizer. PP/PLA blends composites have also been studied to assess the possibility to combine the advantages of the polymers blends and the benefits of polymer composites. In this context, Ebadi-Dehaghani et al. [17] concluded that the addition of two different silicate layers, Cloisite 30B and Cloisite 15A, to the PP/PLA blends decreases the oxygen permeability due to the more tortuous path for diffusion of oxygen molecules.

Among the various classes of films packaging, the antimicrobial packaging has received a great interest due its potential contribution in the removal of harmful organisms and food and devices protection from microbial contamination [22,23]. In this context, copper and its complexes have been found to exhibit a broad-spectrum of biocidal activity and to inhibit the growth of bacteria, fungi, viruses and algae [24–27]. Thus, copper nanoparticles, copper-encapsulated into organic and inorganic compounds and minerals particles supported copper oxides have been dispersed into materials to give them biocidal properties [25]. For polymers, an interesting strategy of incorporating copper and form antimicrobial composites consists in elaborating copper nanoparticle-decorated organically modified montmorillonite (MMT-Cu^{2+}) which suggests the intercalation of copper nanoparticles into the galleries of the nanoclay [26]. This protocol has been envisaged for the development of LDPE/MMT-Cu^{2+} [28] and epoxy/MMT-Cu^{2+} [26] nanocomposites, in which this combined system presents the advantage of being both a reinforcing filler and a bioactive material.

In this study, MMT-Cu^{2+} has been prepared via an ion exchange process. After its characterization to prove the effective intercalation of copper into the MMT, and the confirmation of its antibacterial activity, the modified nanoclay is used to formulate PP/PLA/MMT-Cu^{2+} blend composites with an antimicrobial activity. The thermo-morphological, viscoelastic and environmental properties of PP/PLA/MMT-Cu^{2+} blend composites have been studied as a function of the matrix composition by varying the PP:PLA blends ratios and keeping the MMT-Cu^{2+} at 3 wt.%.

2. Experimental

2.1. Materials

Polypropylene homopolymer, FY4012E (melt flow index (MFI) at 230 °C and under 2.16 kg: 4 g/10 min, density: 0.9 g/cm^3, melting temperature: 159 °C), was purchased from Sumitomo Chemical Asia. PLA is PLI005 resin manufactured by Nature Plast (MFI at 190 °C and under 2.16 kg: 10–30 g/10 min, melting temperature: 155–160 °C). The nanofiller is a sodium bentonite nanoclay (MMT) produced by Sigma Aldrich. Dicumyl peroxide (DCP) and maleic anhydride (MA) were purchased from Sigma-Aldrich to prepare maleic anhydride grafted polypropylene (PP-g-MA) used as a compatibilizer for the PP/PLA blend. Copper sulfate ($CuSO_4$) was purchased from Sigma-Aldrich.

2.2. Processing

2.2.1. Preparation of MMT-Cu^{2+} modified clay

MMT was modified by ion exchange in a $CuSO_4$ solution (0.6 M), mixed at 60 °C for 5 h with stirring. At the end of the reaction, the product was centrifuged at 4000 rpm and the sediment was washed three times with distilled water. The product (MMT-Cu^{2+}) was dried at 80 °C and conserved.

2.2.2. Preparation of blends composites

PP-g-MA was prepared by melt mixing PP with 0.1% of DCP and 3% of MA at 190 °C during 15 min. The evidence of the PP grafting with MA has been provided by Fourier transform infrared spectroscopy (FTIR), which revealed the presence of the carbonyl groups band in the infrared spectra of the modified PP. Before melt blending, PLA, PP-g-MA and MMT-Cu^{2+} were dried at 80 °C for 24 h. PP/PLA blends composites of different compositions (100/0, 90/10, 80/20, 70/30, 60/40, 50/50, 0/100 wt.%) were prepared by incorporating 3 wt.% of MMT-Cu^{2+} and 10 wt.% of PP-g-MA, both referred to the total sample weight. Melt mixing was performed in a Brabender plasticorder, at a mixing speed of 40 rpm and a temperature of 190 °C for 15 min. Table 1 shows the blends composites compositions.

2.3. Characterization

2.3.1. Infrared spectroscopy

FTIR spectra were obtained between 500 and 4000 cm^{-1} on a Perkin Elmer1000. Ten scans were averaged at a resolution of 2 cm^{-1} for the solid tested samples of untreated and copper treated bentonite prepared as KBr pellets (ca. 3% by mass in KBr).

Table 1. Blends composites compositions.

PP/PLA	PP (wt.%)	PLA (wt.%)	PP-g-MA (wt.%)	MMT-Cu^{2+} (wt.%)
100/0	97.0	–	–	3
90/10	74.9	12.1	10	3
80/20	63.8	23.2	10	3
70/30	53.6	33.4	10	3
60/40	44.1	42.9	10	3
50/50	35.4	51.6	10	3
0/100	–	97.0	–	3

2.3.2. X-ray diffraction

X-ray diffraction patterns were recorded at ambient temperature by a Brucker diffractometer, equipped with a CuKα generator operating at a wavelength of 1.5406 Å. The tube current and voltage are 40 mA and 40 kV, respectively. The clays and blends samples used in X-ray diffraction (XRD) measurements were small disks compression molded and hot compressed films, respectively. The measurements were carried out from 2° to 40°. The clay interlayer spacing d was calculated for an order of diffraction n taken equal to the unity, by using Bragg's law:

$$2d\sin\theta = n\lambda$$

λ and θ are, respectively, the X-ray wavelength and the Bragg angle.

2.3.3. Antimicrobial activity

The evaluation of the antimicrobial activity of PLA containing MMT and MMT-Cu^{2+} was carried out by using *Staphylococcus aureus* (gram-positive, ATCC (American Type Culture Collection) 25923). Antimicrobial activity tests were carried out by using the agar disk diffusion method. Film samples were cut into square pieces and placed on Petri dishes containing Mueller–Hinton agar (MHA), previously spread with 0.1 mL of the bacterial culture with a concentration of 10^6 CFU.mL^{-1}, corresponding to the concentration that could be found in contaminated food, and standardized in the McFarland scale 0.5 [29]. The Petri dishes were then incubated at 37 °C for 48 h.

2.3.4. Dynamic mechanical thermal analysis

Rectangular samples of (50 × 10 × 2) mm^3 from PP, PLA and PP/PLA blends composites were used to investigate the temperature-dependent dynamic storage modulus and loss tangent by using a dynamic mechanical thermal analyzer (TA Instruments, Discovery HR-2) operating in shear mode. The temperature range was varied from −40 to 160 °C with a heating rate of 3 °C/min. The samples were scanned at a fixed frequency of 1 Hz with a dynamic strain of 0.01%.

2.3.5. Differential scanning calorimetry

The thermal behavior of the composites was studied on a differential scanning calorimeter (Diamond Differential scanning calorimetry [DSC] from Perkin Elmer). The samples were heated from −50 to 200 °C at a heating rate of 10 °C min^{-1}, kept at 200 °C for 3 min, then cooled to −50 °C at a cooling rate of 10 °C min^{-1}. At last, the samples were heated from −50 up to 200 °C at a heating rate of 10 °C min^{-1}. The analysis was carried out under nitrogen

atmosphere. The PP and PLA crystallinity degrees have been evaluated according to the equation [17]:

$$\chi_c = \frac{\Delta H}{\Delta H_m^0 \left(1 - \left(\frac{\text{wt.\% filler}}{100}\right)\right)} \times 100$$

where $\Delta H = \Delta H_c$ for cooling curves, i.e. the crystallization enthalpy of the sample, or $\Delta H = \Delta H_m - \Delta H_c$ for second heating curves, ΔH_m is the melting enthalpy of the sample and $\Delta H^0{}_m$ the melting enthalpy of the 100% crystalline polymer matrix (201.1 J/g for PP [30] and 93.0 J/g for PLA [31]) and wt.% filler is the total weight percentage of nanoclay and blend component [17].

2.3.6. Scanning electron microscopy

The morphology of the blends composites was studied with a scanning electron microscope (SEM JSM-6301F). SEM micrographs were taken from cryogenically cracked surfaces of the blends specimens after being submerged in liquid nitrogen and fractured immediately. Then, the cross sections of the samples were coated with a conductive gold layer in an automatic sputter coater.

2.3.7. Tensile properties

The tensile strength, Young's modulus and the elongation at break were determined according to ASTM method D412 under ambient conditions, using a tensile testing machine ZwickRoell dynamometer, model Z100. The testing conditions used were: a cross head speed of 1 mm/min and a load cell of 1 N.

2.3.8. Water absorption

Water absorption (WA) was determined using square specimens (20 × 20) mm^2 cut from hot-pressed films. The sample was oven-dried at 40 °C for 24 h, cooled in a desiccator then immediately weighed to obtain the initial weight (W_0). After, the sample is placed in distilled water for 5, 10, 15 and 20 days. After soaking for the specified interval, the sample is removed from water, gently wiped then weighed to get the sample weight after exposure to water absorption (W_t). The sample is placed back in water after each measurement. The percent water absorption was calculated from the following equation [32]:

$$\text{WA}(\%) = \frac{(W_t - W_0)}{W_0} \times 100$$

2.3.9. Biodegradation by soil burial test

Rectangular samples with (30 × 20) mm^2 dimensions were dried until their weights became constant. These samples were then buried in the test soil at a depth of 15–20 cm from the surface for 7 months and irrigated periodically by activated sludge, collected from a municipal wastewater treatment plant, to promote biodegradation. The soil was maintained humid by sprinkling water at regular time intervals. The buried samples were periodically recovered, washed carefully with distilled water, dried then weighted. Biodegradability results were expressed in terms of weight residual percentage (R_w) variations.

3. Results and discussion

3.1. Characterization of modified and unmodified clays

3.1.1. FTIR analysis of MMT and MMT-Cu^{2+}

The unmodified bentonite FTIR spectrum, given in Figure 1, shows in the hydroxyl zone two bands at 3633 and 3431 cm^{-1} corresponding to the stretching vibrations of the Al-OH/Si-OH groups and adsorbed water, respectively. It also reveals a band at 1641 cm^{-1} assigned to the bending in plane vibration of the –OH groups from water. The broad band detected around 1036 cm^{-1} is related to the stretching vibration of the Si–O groups from the tetrahedral components of bentonite, whereas, the Si–O–Al stretching and Si–O–Si bending vibrations are observed at about 519 and 456 cm^{-1} [33,34]. The small bands observed around 2927, 2851 and 1427 cm^{-1} may be due to the presence of organic compounds into the mineral.

After the treatment with $CuSO_4$ solution, the MMT-Cu^{2+} spectra shows a shift of water hydroxyl groups bands of both the stretching vibrations from 3431 to 3487 cm^{-1} and bending vibrations from 1641 to 1636 cm^{-1}. Similar results have been reported by several authors [26,28,35–37] who suggested that the shift of water hydroxyl group bands indicate differently coordinated water forms due to the type of the interlayer cation. The Al-OH and Si-OH vibrations bands are also displaced to 3625 cm^{-1} and their intensity is decreased relatively to the neat MMT, which corroborate with the result reported by Das et al. [26] who proposed that the minimization of the Al–OH band is the proof of the insertion and stabilization of the Cu particles into the interlayer space of the nanoclay. An additional interesting new band is observed at about 3572 cm^{-1} and is related to hydroxyls from the Cu-OH group, confirming the presence of copper into the mineral [33,38].

3.1.2. XRD analysis of MMT and MMT-Cu^{2+}

To endorse the FTIR findings, the XRD patterns of the neat and modified nanoclays are represented in Figure 2. The neat MMT diffractogram displays essentially four peaks at

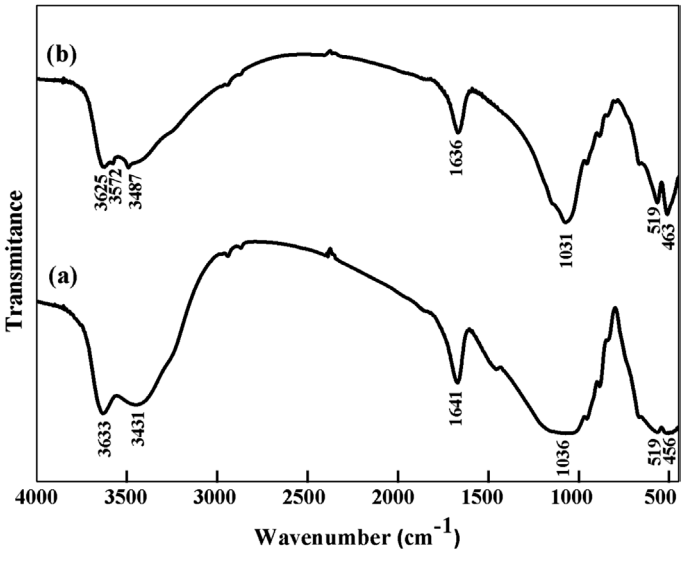

Figure 1. FTIR spectra of: (a) MMT and (b) MMT-Cu^{2+}.

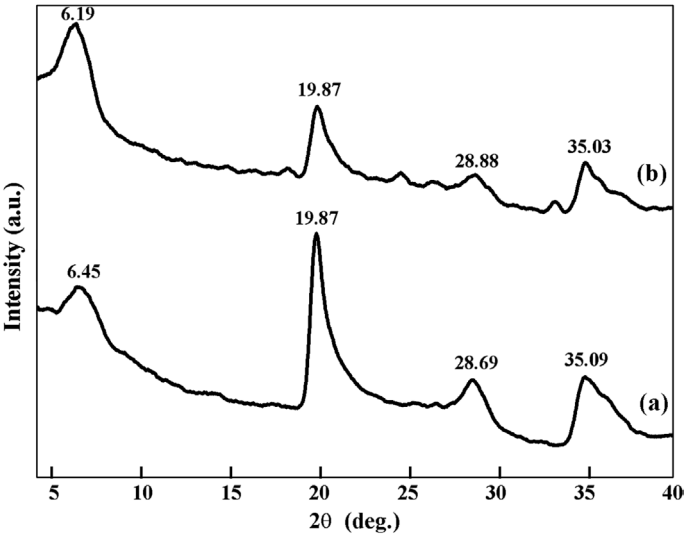

Figure 2. XRD patterns of: (a) MMT and (b) MMT-Cu^{2+}.

2θ of 6.45, 19.87, 28.69 and 35.09°. The peak at 6.45°, corresponding to the basal reflection (0 0 1), is equivalent to an interlayer d-spacing (d_{001}) of 1.37 nm. After the nanoclay treatment with the $CuSO_4$ solution, the diffraction peak of the 001 plane is displaced to 2θ of 6.19° and the interlayer d-spacing is increased to 1.43 nm. The increase in the interlayer distance could be attributed to the Na^+ ion exchange by Cu^{2+}, as it has already been reported by Bruna et al. [28] who noticed an increase of the interlayer gallery from 1.12 to 1.22 nm when inserting copper into MMT. Oueslati et al. [39] studied also the intercalation of Cu^{2+} ions into Wyoming montmorillonite and concluded no additional peaks confirming their presence into the nanoclay, but the authors concluded an increase in the basal space from 1.229 to1.236 nm that they attributed to the copper ions insertion into MMT.

3.1.3. Inhibitory activity of MMT-Cu^{2+}

Figure 3 shows the results of the antimicrobial test performed against *S. aureus* by the agar disk diffusion method, for PLA films prepared without MMT and with 5 wt.% of the unmodified and modified nanoclay. The clear zone formed around the PLA film containing MMT-Cu^{2+} in the media was recorded as an indication of the inhibition of the microbial species. However, no inhibition zone is observed for the PLA film prepared with 5 wt.% of unmodified MMT and the neat PLA film which reveals also an evidence of a microbial degradation beginning. These results demonstrate the antimicrobial action of MMT-Cu^{2+} against *S. aureus*. A similar result has been reported by other authors, who concluded that the antibacterial action of MMT-Cu^{2+} is basically based on copper ion mediated cell disruption which is also significantly promoted by the montmorillonite clay matrix. Indeed, the nanoclay particles do not only serve as stable carriers for the ions but they also increase the contact frequency with the bacterial membrane [40].

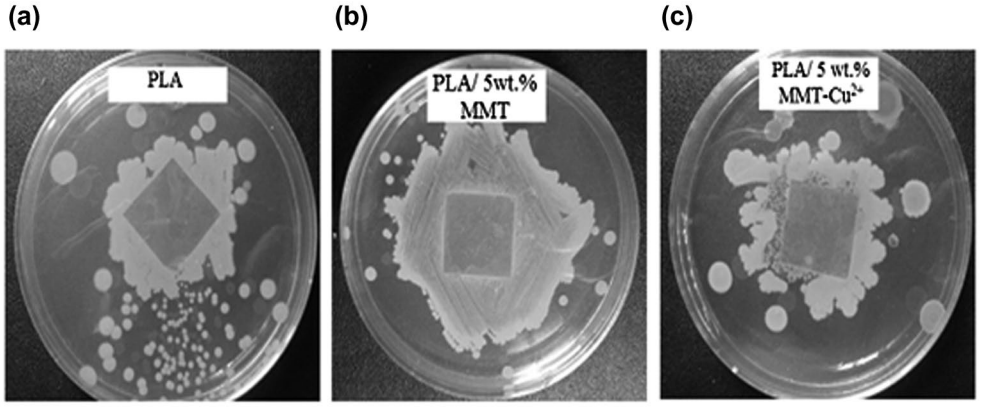

Figure 3. Antimicrobial activity of: (a) PLA film, (b) PLA film with 5 wt.% MMT and (c) PLA film with 5 wt.% MMT-Cu^{2+}.

3.2. Variations of the PP/PLA/MMT-Cu^{2+} composites properties vs. composition

3.2.1. Viscoelastic properties

The viscoelastic behaviors of PP, PLA and PP/PLA blends composites were studied by Dynamic mechanical thermal analysis (DMTA). Plots depicting the variations of the storage modulus G' and the damping factor (tan δ) as a function of temperature for PLA, PP and PP/PLA blends composites are given in Figure 4(a) and (b), respectively. For the PP composite, the storage modulus decreases monotonously over the temperature range due the stiffness decrease of the PP which present a relatively low glass transition temperature (T_g) located around 4 °C. The semi-crystalline state of PP provides a relatively high storage modulus in the temperature range comprised between the glass transition and the melting. On the other hand, the storage modulus of PLA into the PLA composite remains constant over the glassy state, then it decreases sharply around 65 °C as the transition to the rubbery state occurs. After the glass transition, PLA shows an evident increase in the storage modulus because of the increase in the polymer stiffness after the occurring of cold crystallization,

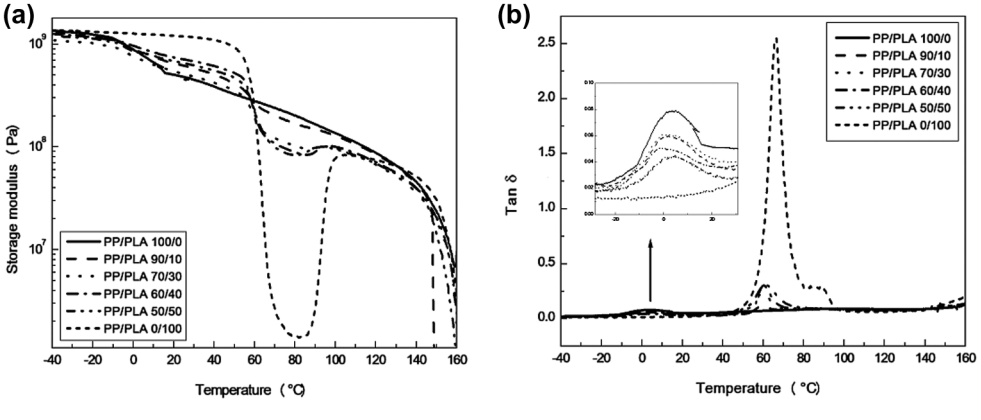

Figure 4. Variations of: (a) storage modulus and (b) tan δ vs. temperature for PP, PLA and PP/PLA blends composites.

resulting from the tendency of the PLA amorphous regions to reorganize into crystallites during heating [9,41,42].

At lower temperatures, the storage moduli of the PP/PLA blends composites do not vary when increasing the temperature and show values that are close to that of the PP composite. As the PP glass transition occurs, the storage moduli decrease is compensated by the relatively high stiffness of the glassy PLA. Moreover, before the PLA glass transition, the blends composites present lower storage moduli than the neat PLA composite due to the low PP stiffness and its plasticizing effect [43]. At the PLA amorphous phase glass transition, the storage moduli of the blends reveal a noticeable drop due to the decrease in the PLA stiffness. But, due to the PP crystalline state, the PP/PLA blends composites present higher storage moduli than the neat PLA composite. Indeed, it is observed that in the temperature range comprised between 63 and 100 °C, the blends composites show storage moduli that depend on the PP concentration; the higher the PP content into the composites, the higher the storage modulus. After the PLA cold crystallization, the storage moduli of the composites decrease obviously due to the approaching of the polymers melting and the significant stiffness decrease for the overall materials.

Figure 4(b) shows the variations of tan δ as a function of temperature for the PP, PLA and PP/PLA blends composites. The maxima in these plots correspond to the structural relaxations in the composites. The main structural relaxation relates to the glass transition of the polymers and its temperature corresponds to their T_g values. The tan δ variations of the homopolymers composites show that only one structural relaxation can be distinguished for each polymer and that the T_g values of PP and PLA appear at about 4 and 66 °C, respectively. In the case of the PP/PLA blends composites, two glass transition peaks are observed for each blend; the higher value corresponds to the PLA component, and the lower one to the PP component. Moreover, the T_g values of both the PLA and PP phases into the blends show no significant shift when the blend composition was varied, which denotes the immiscibility of the two polymers.

3.2.2. Thermal properties

The thermal behaviors of the PP, PLA and the PP/PLA blends composites is studied by examining the DSC thermograms resulting from the first heating, cooling and second heating scans reported in Figure 5(a)–(c), respectively.

The heating curves of PP composite show that PP presents two melting peaks which temperatures taken at the onset are close to 137 and 154 °C and no crystallization peak is detected because of the PP semi-crystalline state owing to its relatively fast crystallization rate [20]. The PP endotherms are attributed, respectively, to the melting of the β- and α-crystals [21].

According to the first heating thermogram of the PLA composite (Figure 5(a)), a small peak superimposed to the glass transition is observed and attributed to the occurrence of physical ageing [41]. The evaluation of the PLA amorphous phase T_g from the second heating thermogram (Figure 5(c)) gives a value of 59 °C. The heating runs (Figure 5(a) and (c)) reveal also a broad peak corresponding to the cold crystallization which temperature (T_c) is taken at the onset around 96 °C, and a double peak related to the melting process and which temperatures are evaluated at about 149 and 155 °C. Several authors have observed the PLA double peak melting behavior and attributed it to the presence of two crystalline phases, namely the pseudo-orthorhombic disordered and orthorhombic ordered structures

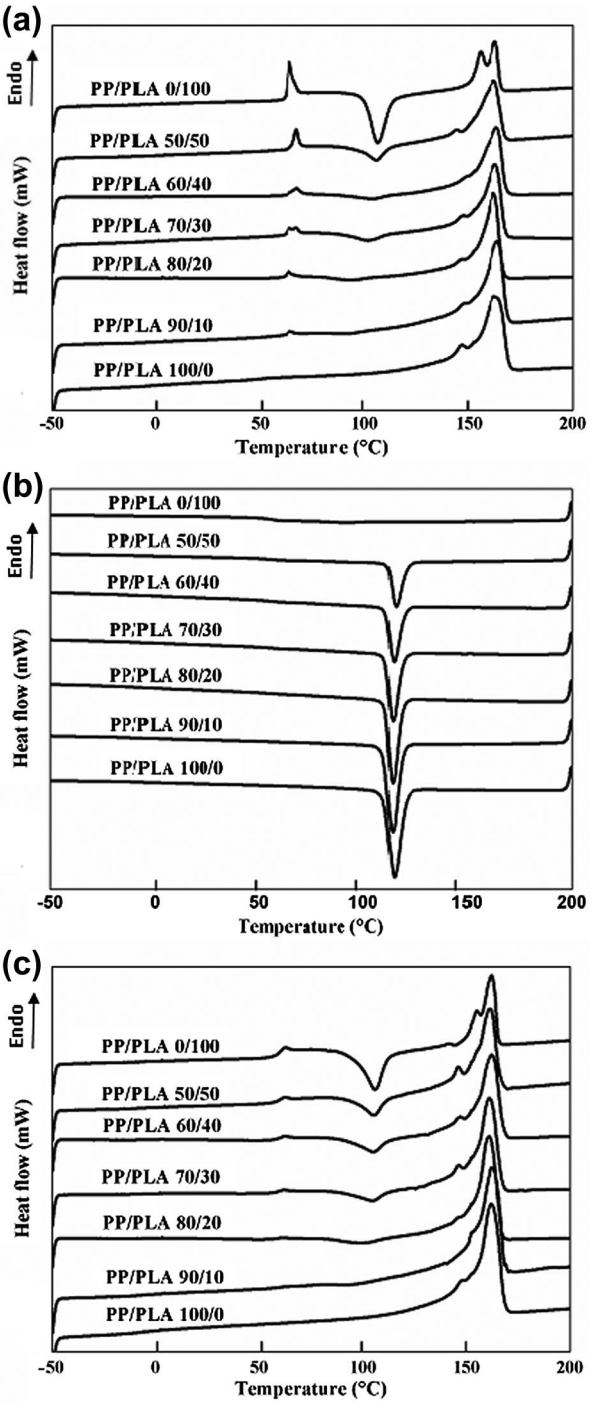

Figure 5. DSC thermograms of the: (a) first heating, (b) cooling and (c) second heating scans of PP, PLA and PP/PLA blends composites.

[44,45]. Additionally, it is noticed that the area of the second peak corresponding to the ordered crystallites is more important which means the larger contribution of this fraction in the melting process of PLA. The evaluation of crystallinity from the second heating scans gives a value of 4% for the PLA composite and 50% for the PP one.

Analogously, the first and second heating scans of the blends composites are similar and reveal small variations of the thermal characteristics (crystallization and melting temperatures) relatively to the homopolymers composites, due to the immiscibility of PP and PLA. The first heating runs show also evidence of PLA physical ageing, allowing the estimation of the T_g from the second heating scans, which point out that blending with PP does not affect the PLA glass transition. The cold-crystallization peak appears in the same temperature range as for the PLA composite and its area seems to be dependent on the PLA contribution into the blends forming the matrix. The blends melting behavior is evidenced by a double peak resulting from the overlapping of the PP and PLA phases endotherms. The first melting peak, which is identical to that observed for the PP composite, may be attributed to the fusion of the β-crystals of the PP phase. However, the second melting peak seems to include the two PLA endotherms and the peak corresponding to the melting of the PP phase α-crystals.

The cooling thermograms (Figure 5(b)) of the PP and PLA composites show quite different aptitude to crystallization. Indeed, PP exhibits a pronounced crystallization peak which temperature at the onset is estimated around 120 °C and the area equivalent to a crystallinity of 48%. In opposite, PLA reveals a little tendency to crystallization that Fukushima et al. [46] explained by its low crystallization rate which prevent the development of a significant crystallinity during the relatively fast cooling process. As a result, PLA attains a crystallinity of only 3%. The cooling thermograms of the PP/PLA blends composites display only the PP melt-crystallization peaks which appear to be displaced to lower temperatures and reveal a higher PP phase crystallinity. The thermal characteristics of PP and PLA into the homopolymers and the blends composites, as determined from the DSC analysis, are summarized in Table 2.

3.2.3. Morphological characterization of PP/PLA/MMT-Cu^{2+}

The morphology evolution for the PP/PLA/MMT-Cu^{2+} blends composites prepared with 3 wt.% of the modified clay is assessed by considering the SEM micrographs represented in Figure 6. The PP's micrograph 6(a) shows a relatively rough surface due to the tough failure of the semi-crystalline morphology. The (70/30) PP/PLA blend's micrograph 6(b) exhibits an irregular dispersion of PLA into the PP matrix and a poor adhesion between the two phases due to their immiscibility. The PLA fraction is segregated into droplets showing diameters comprised between 6.25 and 25 µm. The lack of adhesion between the matrix and the dispersed phase justifies the observed holes resulting from the PLA droplets pulling out from the PP continuous phase during the sample fracturing. The same phase structure is still noticed for the (60/40) PP/PLA blend composite which micrograph 6(c) reveals also an irregular morphology exhibiting PLA droplets with variable diameters. The phase structure adopted by the (70/30) and (60/40) PP/PLA blends composites is due to the PP matrix high viscosity which allows a sufficient shearing intensity favoring the folding of the PLA domains into droplets. The (50/50) PP/PLA blend's composite micrograph 6(d) exhibits a co-continuous morphology where the PP and PLA components form interconnected coarse domains.

Table 2. Thermal characteristics of PP and PLA phases into PP/PLA blends composites as determined from DSC analysis.

		First heating				Cooling			Second heating					
	PP mass fraction	T_{gPLA}	T_{cPLA}	T_{m1}	T_{m2}	T_{cPP}	ΔH_{cPP}	X_{cPP}	T_{gPLA}	T_{cPLA}	ΔH_{cPLA}	T_{m1}	T_{m2}	ΔH_m
PP/PLA	(wt.%)	(°C)	(°C)	(°C)	(°C)	(°C)	(J/g)	(%)	(°C)	(°C)	(J/g)	(°C)	(°C)	(J/g)
100/0	97.0	–	–	137.0	153.0	120.2	94.2	48.3	–	–	–	136.8	153.9	97.4
90/10	74.9	61.6	82.9	138.4	153.9	118.7	96.8	64.2	58.7	86.4	0.3	146.7	153.2	96.8
80/20	63.8	61.8	85.8	136.7	154.0	118.5	77.3	60.2	56.9	84.9	2.7	135.9	153.6	87.0
70/30	53.6	61.8	90.4	139.2	150.4	118.8	73.3	60.8	57.6	95.2	4.3	140.6	153.3	82.3
60/40	44.1	62.1	92.0	138.0	151.0	119.6	56.4	65.0	58.4	93.3	6.9	141.0	153.3	72.5
50/50	35.4	66.9	97.6	135.4	149.0	120.5	48.2	67.7	58.2	95.4	10.2	140.5	153.2	66.3
0/100	0	62.9	98.9	150.4	155.4	–	–	–	58.9	95.6	30.9	149.5	155.5	34.9

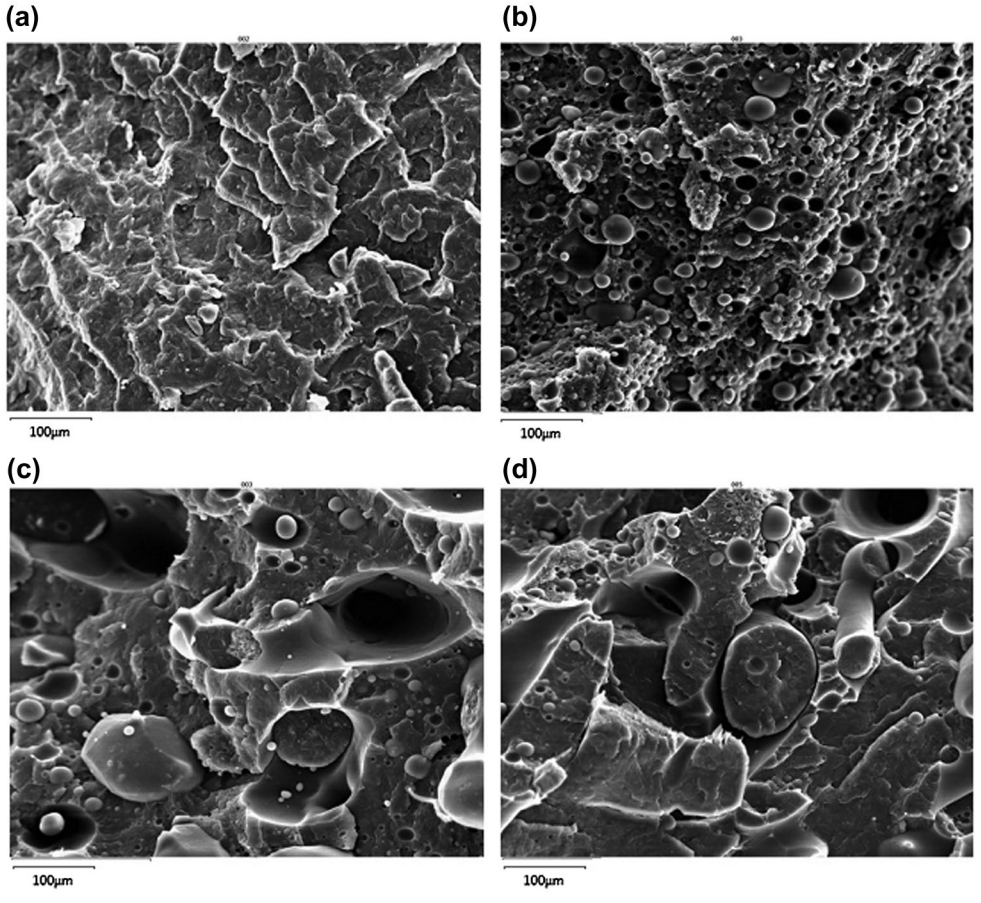

Figure 6. SEM micrographs of PP/PLA/MMT-Cu^{2+} blends composites: (a) 100/0/3, (b) 70/30/3, (c) 60/40/3 and (d) 50/50/3.

The PP composite XRD pattern, represented in Figure 7, exhibits sharp diffraction peaks at 2θ of 13.67°, 16.4°, 18.05°, 20.86° and 21.4° corresponding, respectively, to the (1 1 0), (0 4 0), (1 3 0), (1 1 1) and (0 4 1) lattice planes typical of the monoclinic crystalline form of PP [46]. On the other hand, the PLA composite XRD diagram depicts a broad peak with a maximum at 2θ of 14.4° matching to the 110 plane [47]. It indicates that PLA presents a low crystallinity, as concluded from DSC analysis. The X-ray diagrams of PP/PLA/MMT-Cu^{2+} blends composites, with different PLA contents, are almost identical to that of the PP composite, which indicates that the crystalline structure of these materials is practically governed by the PP α-form crystallites. Identical results have been reported by Lee and Jeong [20]. Also, the presence of MMT-Cu^{2+} into the composites is evidenced by the corresponding diffraction peak which is slightly displaced after blending with PP, PLA and PP/PLA blends.

3.2.4. Tensile properties

The tensile properties of the homopolymers and the blends composites are represented in Figure 8(a)–(d). Due to its higher stiffness at ambient temperature, the PLA composite presents a higher tensile strength and Young's modulus than those of the PP one. In opposite,

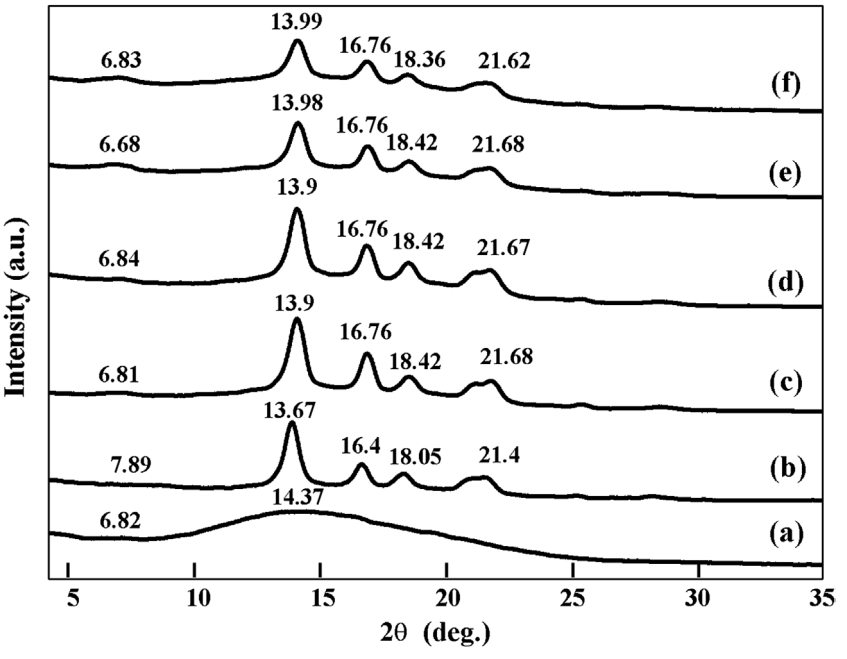

Figure 7. XRD diagrams of: (a) PLA, (b) PP and (c) (80/20), (d) (70/30), (e) (60/40) and (f) (50/50) PP/PLA blends composites prepared with 3 wt.% of MMT-Cu^{2+}.

the PP composite exhibits a higher deformation at break. For the PP/PLA/MMT-Cu^{2+} composites, the tensile strength decreases with increasing the PLA content. This could be ascribed to the lack of adhesion resulting from the blend phase separation, as observed from SEM micrographs. This kind of behaviors where the tensile strength of a blend is lower than the strength values of its pure components is typical of immiscible systems. Also, the increase in Young's modulus and the decrease in the elongation at break indicate a transition from a ductile to a brittle behavior as the PLA contribution into the blend increases. This transition is explained by the fact that PLA has a lower elongation at break compared to PP and by the incompatibility of the two polymers, which implies that during the loading, PP/PLA matrix breaks up for lower deformations and before the PP domains stretch fully, due to the lack of stress transfer at the interface between the two components.

3.3. Environmental properties of PP/PLA/MMT-Cu^{2+} blends composites

3.3.1. Water absorption

Water absorption by PLA and (50/50) PP/PLA blend and their composites are represented in Figure 9. On the contrary of the PP hydrophobic feature which does not allow water absorption, the relatively PLA significant hydrophilic nature is due to the great tendency of its terminal polar groups to attract water molecules. (50/50) PP/PLA blend exhibits an intermediate water resistance behavior, and after 15 days of immersion, it is noticed that water absorption of PP/PLA blend is equivalent to that of PP. This result is probably due to the contribution of the PP hydrophobic nature and to the co-continuous morphology of the (50/50) PP/PLA blend, which probably reduces the water diffusion path through the blend.

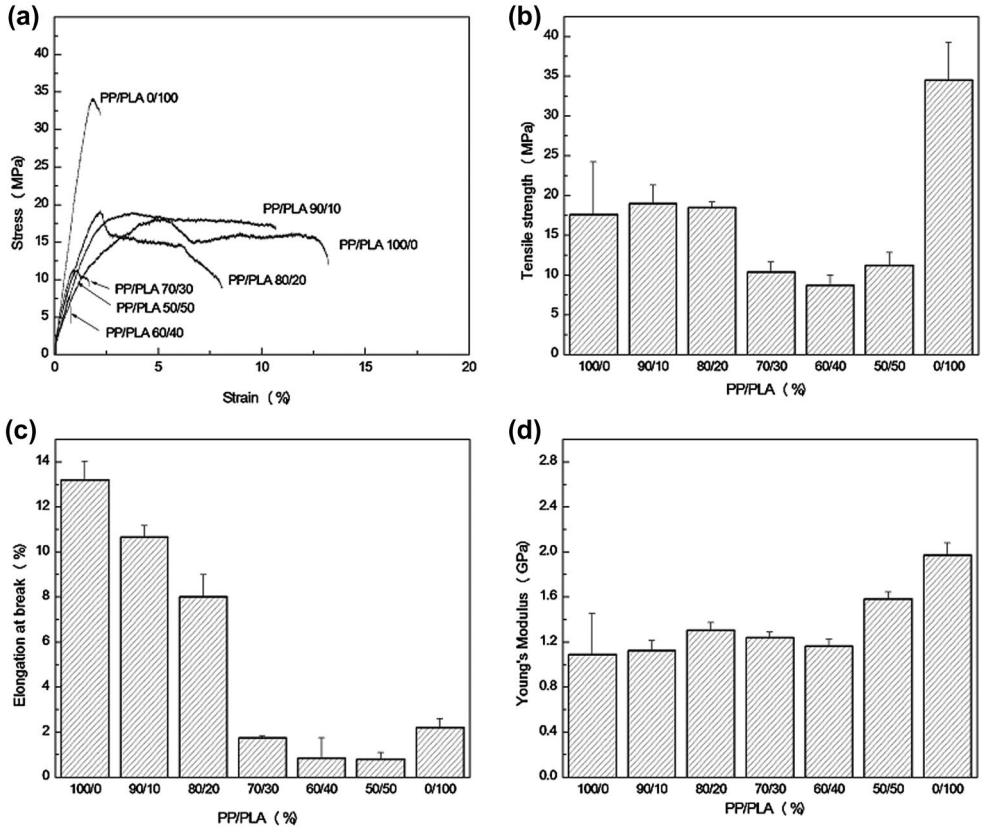

Figure 8. Tensile properties of PP/PLA/MMT-Cu^{2+} blends composites prepared with 3 wt.% of MMT-Cu^{2+}: (a) Stress-strain curves, (b) Tensile strength, (c) Elongation at break, (d) Young's modulus.

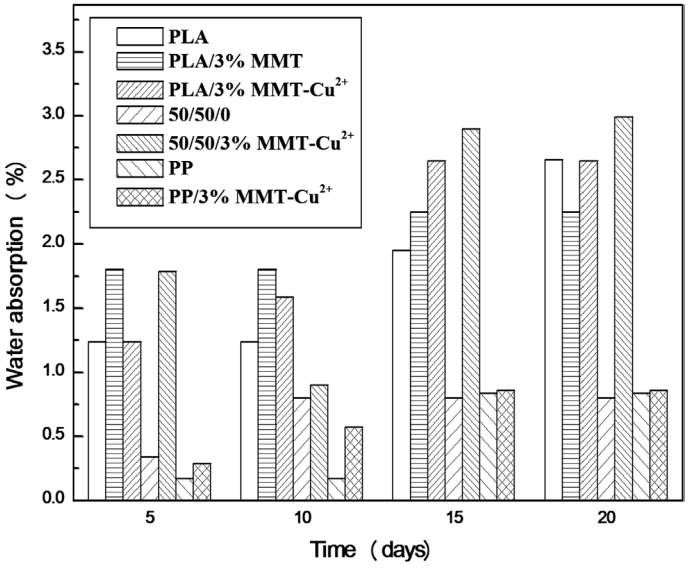

Figure 9. Variations of water absorption for PLA and (50/50) PP/PLA blend and their composites as a function of immersion time.

Additionally, PLA and (50/50) PP/PLA blend composites reveal a much important WA when compared to the neat samples. Indeed, MMT particles show a high hydrophilic aptitude due to the presence of hydratable cations in the interlayer galleries [48]. It is worth mentioning that for much longer immersion time, the PLA composite WA percentage is more important in presence of MMT-Cu^{2+} than for the composite containing the neat MMT. Such interesting result could be explained by the fact that the intercalation of copper ions causes noticeable changes in the hydrophilic nature of the clay mineral, as it has been pointed out by FTIR analysis, which could result from the increase in the clay interlayer distance after Na^{+} ions exchanging by Cu^{2+} ones. Accordingly, the larger the interlayer distance of the nanoclay, the higher the composite water absorption aptitude.

3.3.2. Biodegradability assessment

Figure 10 represents the variations of the residual weight percentages of PP, PLA, (50/50) PP/PLA blend and their composites vs. burial time. PP films reveal no weight loss due to its main chains bio-resistance resulting from the involvement of only carbon atoms and the absence of hydrolysable functional groups. Oppositely, the neat PLA films show a sharp weight loss after approximately four months which is the PLA critical time to start heterogeneous hydrolysis. The hydrolysis reaction is the main reaction which leads to the beginning of the PLA degradation through a fragmentation process. Indeed, the degradation of PLA is carried out in two stages. During the initial phase, the high molecular weight PLA chains are hydrolyzed to form lower molecular weight chains. In the second step, the microorganisms in the environment continue the degradation process by converting these lower molecular weight components to carbon dioxide, water, and humus [49].

On the other hand, PP/PLA blend does not show degradation during the study period. This can be explained by the non-degradability of the PP phase and by the relatively low water absorption rate of the material. This could prevent hydrolysis reactions necessary for

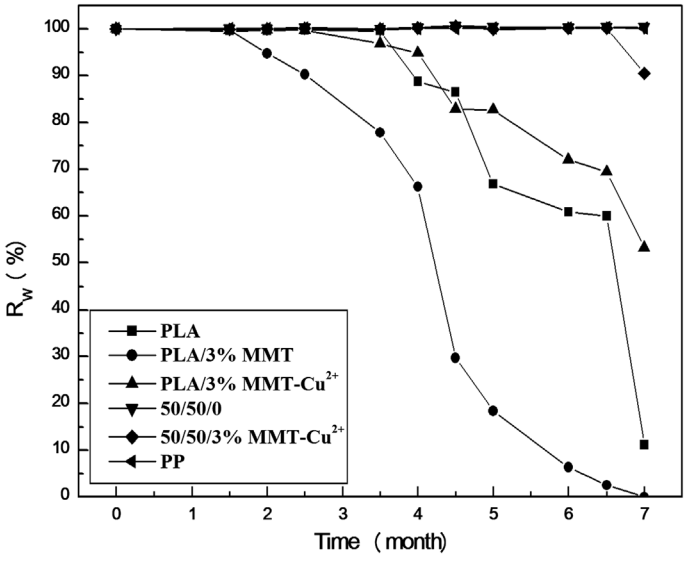

Figure 10. Time-dependence of weight residual percentage for PP, PLA, (50/50) PP/PLA blend and their composites.

the sample fragmentation and the diffusion of the microorganisms, such as bacteria and fungi, from the degrading medium to the interior of the matrix using water as a vehicle.

The biodegradability of the neat PLA and PP/PLA blend is enhanced after the nanoclay incorporation. In this context, several authors [48,50,51] supported the conclusion of the nanoclay's catalytic effect on the biodegradation of PLA and its blends and justified that clay interfaces constitute a suitable diffusion path for the microorganisms and the desired medium for their growth due to the mineral hydrophilic nature. Consequently, samples with higher water absorption are usually more prone to microorganism attack [52]. However, it is observed that although the higher water absorption rate of the PLA/MMT-Cu^{2+} composite, its tendency to biodegradation is notably lower to that of the composite PLA/MMT. This can be due to antimicrobial activity of Cu^{2+}-exchanged MMT which inhibits the attack of the composite by bacteria. Additionally, even the catalytic effect exerted by the MMT on the PLA phase biodegradation, the (50/50) PP/PLA blend composite still present no tendency for biodegradation over 6 months, even the high water absorption ability. Thus, the incorporation of PLA and MMT-Cu^{+2} to PP, should offer the opportunity for obtaining, from a biodegradable polymer, a more resistant and antimicrobial material that could find an issue in the packaging domain.

4. Conclusion

In this study, the thermo-mechanical, viscoelastic, morphological and environmental properties of the PP/PLA blends composites have been investigated as a function of the blend composition after the addition of 3% of a modified nanoclay MMT-Cu^{2+} obtained from an ion exchange process of Na^{+} ions by Cu^{2+} ones.

The characterization of the modified MMT by FTIR analyses revealed variations in the hydroxyl zone which is the proof of differently coordinated water forms due to the type of the interlayer cation. This result has been supported by the XRD analyses which showed a shift of the 0 0 1 diffraction peak of the nanoclay and an increase in the basal space. An additional evidence of the presence of copper ions into the mineral is provided by the inhibitory activity against the bacterial growth revealed by the PLA composites.

The viscoelastic characterization revealed that after the PP glass transition, the high PLA stiffness increases the storage modulus of the blends composites. Likewise, after the PLA glass transition, the PP crystalline phase promotes the composites storage modulus which increases as the PLA contribution into the blends decreases. The variations of tan δ showed that the glass transition temperatures of PP and PLA did not vary with the composition of the blends and after the addition of MMT-Cu^{2+}.

Additionally, the thermal characteristics of the PP and PLA phases into the blends composites exhibited small variations relatively to the homopolymers ones. Also, the tensile properties showed that the incorporation of PLA induces significant variations on the PP mechanical properties by increasing the Young's modulus and decreasing the elongation at break.

Due to the larger interlayer space of the MMT-Cu^{2+} clay, the (50/50) PP/PLA blend composite exhibited a high water absorption aptitude relatively to the neat blend. Although the proved catalytic role of the clay minerals on the biodegradation process of biopolymers, the (50/50/3) PP/PLA/MMT-Cu^{2+} composite exhibited an adequate bio-resistance even though the severe degrading medium to which it was exposed.

Disclosure statement

No potential conflict of interest was reported by the authors.

ORCID

Nacerddine Haddaoui http://orcid.org/0000-0002-1515-0867

References

[1] Nampoothiri KM, Nair NR, John RP. An overview of the recent developments in polylactide (PLA) research. Bioresour Technol. 2010;101:8493–8501.
[2] Schreck KM, Hillmyer MA. Block copolymers and melt blends of polylactide with Nodax™ microbial polyesters: preparation and mechanical properties. J Biotechnol. 2007;132:287–295.
[3] Auras R, Harte B, Selke S. An overview of polylactides as packaging materials. Macromol Biosci. 2004;4:835–864.
[4] Auras RA, Singh SP, Singh JJ. Evaluation of oriented poly(lactide) polymers vs. existing PET and oriented PS for fresh food service containers. Packag Technol Sci. 2005;18:207–216.
[5] Vainionpää S, Rokkanen P, Törmälä P. Surgical applications of biodegradable polymers in human tissues. Prog Polym Sci. 1989;14:679–716.
[6] Paul DR, Newman S. Polymer blends. New York (NY): Academic press; 1978.
[7] Abdelwahab MA, Flynn A, Chiou BS, et al. Thermal, mechanical and morphological characterization of plasticized PLA-PHB blends. Polym Degrad Stab. 2012;97:1822–1828.
[8] Engelberg I, Kohn J. Physico-mechanical properties of degradable polymers used in medical applications: a comparative study. Biomaterials. 1991;12:292–304.
[9] Djellali S, Sadoun T, Haddaoui N, et al. Viscosity and viscoelasticity measurements of low density polyethylene/poly(lactic acid) blends. Polym Bull. 2015;72:1177–1195.
[10] Singh G, Kaur N, Bhunia H, et al. Degradation behaviors of linear low-density polyethylene and poly(L-lactic acid) blends. J Appl Polym Sci. 2012;124:1993–1998.
[11] Hashima K, Nishitsuji S, Inoue T. Structure-properties of super-tough PLA alloy with excellent heat resistance. Polymer. 2010;51:3934–3939.
[12] Ayana B, Suin S, Khatua BB. Highly exfoliated eco-friendly thermoplastic starch (TPS)/poly(lactic acid) (PLA)/clay nanocomposites using unmodified nanoclay. Carbohydr Polym. 2014;110:430–439.
[13] Malwela T, Ray SS. Study of morphology and crystal growth behaviour of nanoclay-containing biodegradable polymer blend thin films using atomic force microscopy. Polymer. 2012;53:2705–2716.
[14] Jiang L, Wolcott MP, Zhang JW. Study of biodegradable polylactide/poly(butylene adipate-co-terephthalate) blends. Biomacromolecules. 2006;7:199–207.
[15] Rohlmann CO, Failla MD, Quinzani LM. Linear viscoelasticity and structure of polypropylene–montmorillonite nanocomposites. Polymer. 2006;47:7795–7804.
[16] Pasquini N. Polypropylene handbook. 2nd ed. Cincinnati (OH): Hanser Gardner Publications; 2005.
[17] Ebadi-Dehaghani H, Barikani M, Khonakdar HA, et al. On O_2 gas permeability of PP/PLA/clay nanocomposites: a molecular dynamic simulation approach. Polym Test. 2015;45:139–151.
[18] Yoo TW, Yoon HG, Choi SJ, et al. Effects of compatibilizers on the mechanical properties and interfacial tension of polypropylene and poly(lactic acid) blends. Macromol Res. 2010;18:583–588.
[19] Pivsa-Art S, Kord-Sa-Ard J, Pivsa-Art W, et al. Effect of compatibilizer on PLA/PP blend for injection molding. Energy Procedia. 2016;89:353–360.
[20] Lee TW, Jeong YG. Enhanced electrical conductivity, mechanical modulus, and thermal stability of immiscible polylactide/polypropylene blends by the selective localization of multi-walled carbon nanotubes. Compos Sci Technol. 2014;103:78–84.

[21] Lei F, Yu H, Yang S. Analysis of crystalline structure and morphology of isotactic polypropylene under the coexistence of organic montmorillonite particles and shear flow. Polymer. 2016;82:274–284.
[22] Tankhiwale R, Bajpai SK. Preparation, characterization and antibacterial applications of ZnO-nanoparticles coated polyethylene films for food packaging. Colloid Surf B: Biointerfaces. 2012;90:16–20.
[23] Xing Y, Li X, Zhang L, et al. Effect of TiO_2 nanoparticles on the antibacterial and physical properties of polyethylene-based film. Prog Organic Coatings. 2012;73:219–224.
[24] Shukla PB, Mishra M, Dave S, et al. A study on antimicrobial activity of silica supported copper oxide against *Escherichia coli*. Int J Front Sci Technol. 2014;2:1–13.
[25] Rubilar O, Rai M, Tortella G, et al. Biogenic nanoparticles: copper, copper oxides, copper sulphides, complex copper nanostructures and their applications. Biotechnol Lett. 2013;35:1365–1375.
[26] Das G, Kalita RD, Gogoi P, et al. Antibacterial activities of copper nanoparticle-decorated organically modified montmorillonite/epoxy nanocomposites. Appl Clay Sci. 2014;90:18–26.
[27] Jia B, Mei Y, Cheng L, et al. Preparation of copper nanoparticles coated cellulose films with antibacterial properties through one-step reduction. Appl Mater Interfaces. 2012;4:2897–2902.
[28] Bruna JE, Peñaloza A, Guarda A, et al. Development of $MtCu^{2+}$/LDPE nanocomposites with antimicrobial activity for potential use in food packaging. Appl Clay Sci. 2012;58:79–87.
[29] Ramos M, Jiménez A, Peltzer M, et al. Characterization and antimicrobial activity studies of polypropylene films with carvacrol and thymol for active packaging. J Food Eng. 2012;109:513–519.
[30] Bai F, Li F, Calhoun B, et al. Polymer handbook. 4th ed. New York (NY): Wiley; 1999.
[31] Brandrup J, Immergut EH. Polymer handbook. New York (NY): Wiley; 1975.
[32] Arjmandi R, Hassan A, Haafiz MKM, et al. Effect of hydrolysed cellulose nanowhiskers on properties of montmorillonite/polylactic acid nanocomposites. Int J Biol Macromolec. 2016;82:998–1010.
[33] Chen ZY, Persson D, Nazarov A, et al. *In situ* studies of the effect of CO_2 on the initial NaCl-induced atmospheric corrosion of copper. J Electrochem Soc. 2005;152:B342–B351.
[34] Saikia BJ, Parthasarathy G. Fourier transform infrared spectroscopic characterization of kaolinite from Assam and Meghalaya, Northeastern India. J Mod Phys. 2010;1:206–210.
[35] Hundakova M, Valaskova M, Tomasek V. Silver and/or copper vermiculites and their antibacterial effect. Acta Geodyn Geomater. 2013;10:97–104.
[36] Kloprogge JT, Mahmutagic E, Frost RL. Mid-infrared and infrared emission spectroscopy of Cu-exchanged montmorillonite. J Colloid Interface Sci. 2006;296:640–646.
[37] Sarier N, Onder E, Ersoy S. The modification of Na-montmorillonite by salts of fatty acids: an easy intercalation process. Colloid Surf A: Physicochem Eng Asp. 2010;371:40–49.
[38] Zhang YX, Huang M, Li F, et al. Controlled synthesis of hierarchical CuO nanostructures for electrochemical capacitor electrodes. Int J Electrochem Sci. 2013;8:8645–8661.
[39] Oueslati W, Benrhaiem H, Lanson B, et al. Selectivity of Na–montmorillonite in relation with the concentration of bivalent cation (Cu^{2+}, Ca^{2+}, Ni^{2+}) by quantitative analysis of XRD patterns. Appl Clay Sci. 2009;43:224–227.
[40] Bagchi B, Kar S, Dey SK, et al. *In situ* synthesis and antibacterial activity of copper nanoparticle loaded natural montmorillonite clay based on contact inhibition and ion release. Colloids Surf B: Biointerfaces. 2013;108:358–365.
[41] Pluta M, Murariu M, Alexandre M, et al. Polylactide compositions. The influence of ageing on the structure, thermal and viscoelastic properties of PLA/calcium sulfate composites. Polym Degrad Stab. 2008;93:925–931.
[42] As'habi L, Jafari SH, Khonakdar HA, et al. Non-isothermal crystallization behavior of PLA/LLDPE/nanoclay hybrid: synergistic role of LLDPE and clay. Thermochim Acta. 2013;565:102–113.
[43] Kang H, Lu X, Xu Y. Properties of immiscible and ethylene-butyl acrylate-glycidyl methacrylate terpolymer compatibilized poly (lactic acid) and polypropylene blends. Polym Test. 2015;43:173–181.

[44] Zhang JM, Tashiro K, Tsuji H, et al. Disorder-to-order phase transition and multiple melting behavior of poly(L-lactide) investigated by simultaneous measurements of WAXD and DSC. Macromolecules. 2008;41:1352–1357.
[45] Yasuniwa M, Tsubakihara S, Iura K, et al. Crystallization behavior of poly(l-lactic acid). Polymer. 2006;47:7554–7563.
[46] Aslanzadeh S, Haghighat Kish M, Katbab AA. Effects of melt processing conditions on photo-oxidation of PP/PPgMA/OMMT composites. Polym Degrad Stab. 2010;95:1800–1809.
[47] Fukushima K, Tabuani D, Arena M, et al. Effect of clay type and loading on thermal, mechanical properties and biodegradation of poly(lactic acid) nanocomposites. React Funct Polym. 2013;73:540–549.
[48] Zhou Q, Xanthos M. Nanoclay and crystallinity effects on the hydrolytic degradation of polylactides. Polym Degrad Stab. 2008;93:1450–1459.
[49] Kolstad J, Vink E, De Wilde B, et al. Assessment of anaerobic degradation of Ingeo (TM) polylactides under accelerated landfill conditions. Polym Degrad Stab. 2012;97:31–41.
[50] Maiti P, Batt CA, Giannelis E. Renewable plastics: Synthesis and properties of PHB nanocomposites. Polym Mater Sci Eng. 2003;88:58–59.
[51] Medjdoub N, Guessoum M, Fois M. Viscoelastic, thermal and environmental characteristics of poly(lactic acid), linear low-density polyethylene and low-density polyethylene ternary blends and composites. J Adhes Sci Technol. 2016;31:787–805.
[52] Chuatjuljit S, Hosililak S, Athisart A. Thermoplastic cassava starch/sorbitol-modified montmorillonite nanocomposites blended with low density polyethylene: properties and biodegradability study. J Metals Mater Miner. 2009;19:59–65.